Hindawi
Journal of Spectroscopy
Volume 2019, Article ID 6043523, 6 pages
https://doi.org/10.1155/2019/6043523

Research Article

Microscopy and Spectroscopy Characterization of Carbon Nanotubes Grown at Different Temperatures Using Cyclohexanol as Carbon Source

Elsa G. Ordoñez Casanova,[1] **Héctor A. Trejo Mandujano**,[1] **and Manuel Román Aguirre**[2]

[1]*Universidad Autónoma de Ciudad Juárez, Av. del Charro no. 450 Nte. Col. Partido Romero CP 32310, Ciudad Juárez, Chihuahua, Mexico*
[2]*Centro de Investigación de Materiales Avanzados S.C., Miguel de Cervantes 120, Complejo Industrial Chihuahua, 31109 Chihuahua, Chihuahua, Mexico*

Correspondence should be addressed to Héctor A. Trejo Mandujano; htrejo@uacj.mx

Received 3 February 2019; Revised 24 April 2019; Accepted 10 July 2019; Published 14 August 2019

Academic Editor: K.S.V. Krishna Rao

We present the structural and spectroscopy characterization of carbon nanotubes (CNTs) grown by the spray pyrolysis technique, using ferrocene as catalyzer and cyclohexanol as the carbon source, and synthetized in a temperature range of 750 to 1000°C. The structural morphology was observed using scanning electron microscopy (SEM) and transmission electron microscopy (TEM). The spectroscopy response was obtained by UV-Vis and Raman spectroscopy. We observed morphological changes and found that the product yield seems to increase with temperature. The optical characterization corroborated the presence of $n-\pi^*$ transitions and Van Hove singularities as result of possible electrical conductivity changes.

1. Introduction

Nowadays, the search for growth methods to obtain CNTs at low cost and with high quality is very important for their industrial applications [1]. This task can be accomplished by modifying the parameters that affect growth such as temperature, carbon sources, metal seed source or catalyst, and growing time [2, 3]. As verified experimentally, obtaining a desired structural quality and/or purity in the nanotubes is considered important since it directly influences their physical and chemical properties [4–6].

Thermally decomposed hydrocarbon vapors at low temperatures (700–750°C), in conjunction with metal oxide catalyst particles as "seeds" for the CNT growth, have been frequently used as carbon source during chemical vapor deposition. The specific type of source used has a direct influence on the final product characteristics. For example, the use of alcohols yields few-wall carbon nanotube, and the number of carbons in aliphatic alcohols affects the CNT's microstructure [7]. Other sources like aromatic compounds are well known to produce well-aligned, pure, and long multiwall carbon nanotube (MWCNT) forest. Also, the product from these sources normally results in high number of walls and large outer diameter [8].

In this context, cyclohexanol has attracted the attention of several authors due to its cyclical structure and boiling temperature [7–10]. The effects of syntheses using cyclohexanol [11] as carbon source have been presented in some publications. For instance, Shirazi et al. used this compound at a fixed temperature of 750°C and found improved properties (crystallinity and growth) accredited to the oxygen helping eliminate amorphous carbon by oxidation [9]. In other studies, Liu et al. used Co in their process and observed catalytic activity in the selective dehydrogenation of cyclohexanol to cyclohexanone. They present the performance and influence of this catalyst in the structural and

electronic properties of the CNTs [10]. Finally, Musso et al employed cyclohexanol at the low temperature of 650°C to corroborate the growth of carbon nanotubes over silicon wafers [8].

In this work, we compared the morphological structure and the optical spectroscopic behavior of CNTs grown by the alternate method of spray pyrolysis using cyclohexanol as carbon source and ferrocene as catalyzer at a fixed ratio, varying only the synthesis temperature (750, 800, 850, 900, and 1000°C). This study allows us to find the most suitable temperature range for this technique, under the specified synthesis parameters, in order to obtain CNTs with good structural morphology, chirality type, and optical characteristics.

2. Materials and Methods

Using the vapor pyrolysis technique [7], we employed a ferrocene/cyclohexanol mix at a ratio of 0.20 g/20 ml introduced at a rate of 1 mL/min during 20 min; the obtained vapor was carried by argon flow at 0.32 L/min to a quartz tube (substrate) inside the furnace. Using the above parameters for all the experiments, we made syntheses at 750, 800, 850, 900, and 1000°C. The technique controls the reactant input, but it does not account for the characteristics of the residues that are expelled out as fumes. At the end of each synthesis, the obtained product was recollected by scraping the central part of the quartz tube, the yield was weighed, and then the samples were prepared for characterization.

2.1. Characterization. Morphology and microstructural characterization of the CNTs were observed by scanning electron microscopy (SEM) in a JSM-7401F instrument operated at 3–5 kV and by high-resolution transmission electron microscopy (HRTEM) in a JEOL JEM-2100FS with beam Cs-corrector operated at 200 kV and spatial resolution close to 0.13 nm. The Raman spectra were acquired by the LabRam Horiba HR system using a He-Ne laser at 632.8 nm and 14.2 mW equipped with a CCD detector column at −75°C. The resolution obtained was of approximately 1 cm^{-1}. Finally, the UV-Vis spectra were collected using a Cary 100 spectrophotometer (Varian Corp.) (190–1100 nm, ±1 nm, 0.5 nm).

3. Results and Discussion

3.1. Yield Dependence of Temperature. The first observation was that the product yield increased with temperature, obtaining a product of 0.20 g for the lowest temperature and 0.55 g for the highest temperature. The low CNT formation can be explained due to low temperature and high gas flow: under these conditions, not all the hydrocarbons reach the pyrolysis temperature and leave the furnace without decomposing to elemental carbon, iron, and hydrogen. This result agrees with previous reports [12].

3.2. SEM Characterization. Figures 1(a)–1(e) show SEM images that reveal the variation of microstructural CNTs as a function of temperature. We can observe an important amount of iron nanoparticles of different sizes for the two lower temperatures of 750 and 800°C. CNTs obtained at 800°C seem to be short and with small diameter compared to those obtained at 850°C or higher temperatures. The images for 850 and 900°C show well-defined CNTs of different diameters, and at 900°C, significantly fewer iron nanoparticle impurities were present. Products at 1000°C show less CNTs formation and more graphitic carbon.

3.3. Characterization. Figures 2(a)–2(d) show TEM images for the 750, 800, 900, and 1000°C cases. The TEM image of 750°C CNTs displays inhomogeneous structure and it was not possible to measure the diameter. Image for 800°C clearly displays how the iron nanoparticle promotes the graphite walls around it constituting the structure of the CNTs [13–15]. It was confirmed that the formed CNTs were present with a few walls (MWCNTs) and showed a homogeneous structure. For the lower and higher temperatures, the organization of the graphite walls is compromised, the sizes of the iron nanoparticle impurities increase, and the few-wall CNTs present high structural defects [15, 16]. This behavior can be contrasted to the use of aromatic compounds, where to the best of our knowledge, no one has reported the reason why they lead better product than alcohols. One possibility is that the sp^2 hybridization on the structure of aromatic sources makes it easier for the graphene to form cylindrical layers. The sp^3 hybridization on aliphatic alcohols or cyclohexanol makes the formation of cylindrical graphene difficult and the restructuring of solid carbon leads to shortest, low wall number CNTs, with graphitic carbon formation. These circumstances affect the crystallinity as shown.

Finally, the results from TEM analyses show an average distribution variety of external diameter (7 nm–12 nm) and a thickness range of the iron nanoparticles (9 nm–25 nm).

3.4. Raman Characterization. Figure 3 shows the Raman characterization of the six samples. According to the literature, the peak at 1340 cm^{-1} is assigned to the poorly organized residual graphite [17, 18]. In this region, the peak is related to the so-called D band (band disorder) [19, 20]. The frequencies between 1500 cm^{-1} and 1600 cm^{-1} are related to the G band and are highly related to the characteristic of single- and multiple wall nanotubes. These frequencies correspond to a splitting of the graphite extension mode (stretching mode) [7, 13–16]. A second-order vibration mode between 2450 cm^{-1} and 2650 cm^{-1} is assigned to the first on-tone mode and to the D mode, also called G' (2D) [21, 22].

The results of the Raman spectrum present response from 500 to 3000 cm^{-1}, in which the characteristic D band and G band peaks are observed. The D band lies between 1330 cm^{-1} to 1333 cm^{-1} and the G band between 1582 cm^{-1} and 1596 cm^{-1} for. For the 750 and 1000°C cases, the D peaks are higher than their G counterpart meaning that the sp^2 bonds are broken [23], indicating there are more sp^3 bonds and there is a presence of poorly organized graphite in our samples, as shown in the SEM

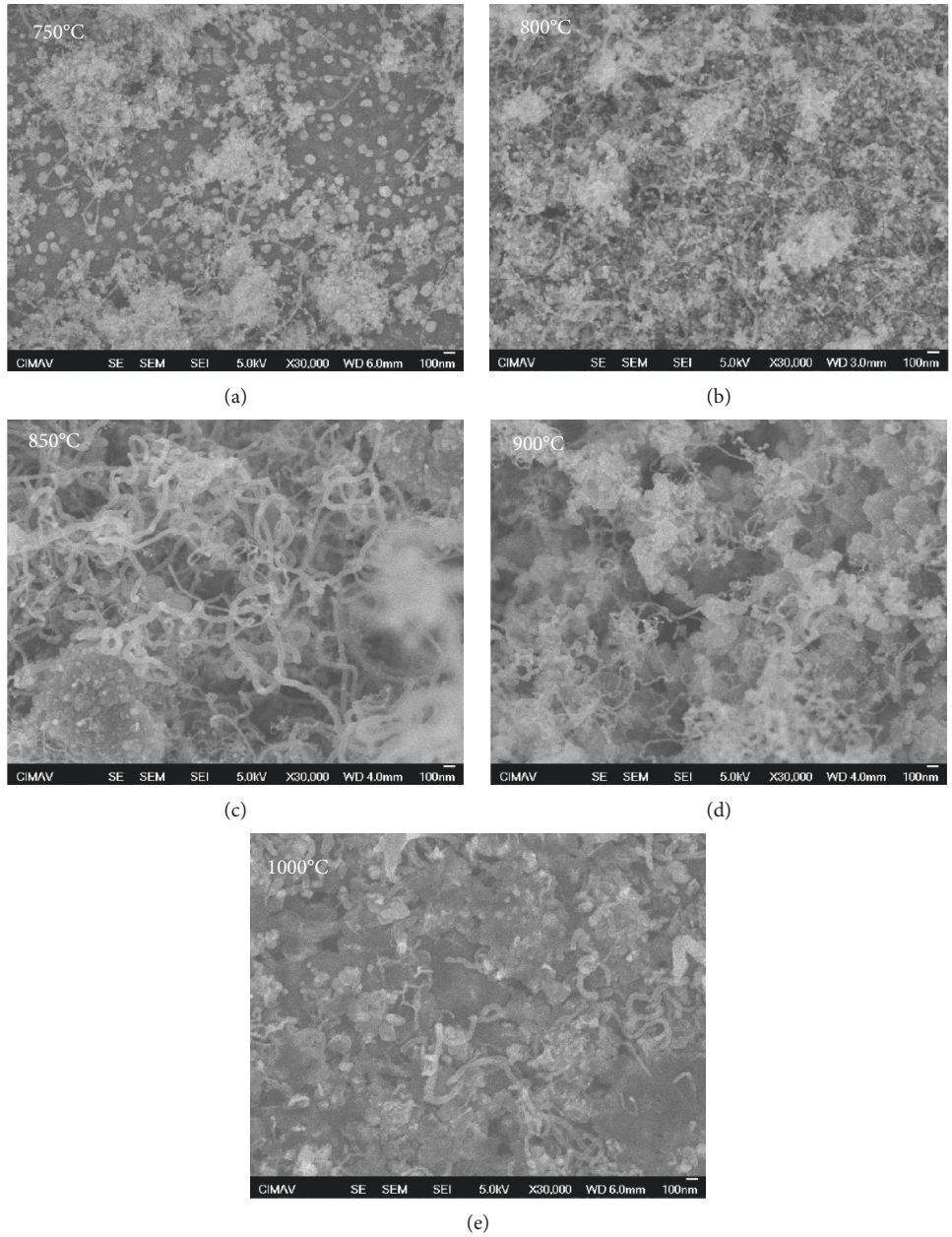

Figure 1: SEM images of CNTs (a) at 750°C, (b) at 800°C, (c) at 850°C, (d) at 900°C, and (e) at 1000°C.

and TEM characterization. The intensity ratio ID/IG, between 0.83 and 0.84 for all cases, means that all the samples contain defects on their CNTs [23]. However, for the samples of 850 and 900°C, the intensity of the D band is lower than that of the samples of other temperatures, indicating the product with less structural defects.

The 2D band lies between 2440 and 2650 cm^{-1}, which is the second-order harmonic of the 2D band and is associated with the degree of crystallinity of the graphitic layers. The G' band is most intense for few-wall CNTs and it gets lower as the number of walls increases. Also, the ratio I2D/IG increases as the number of layers decreases [23]. Our samples showed well-defined 2D band for only three cases (800, 850, and 900°C) and a I2D/IG ratio of 0.59–0.60 for all cases, indicating the presence of MWCNTs.

3.5. UV-Vis. Figure 4 shows the UV-Vis spectra of MWCNTs for each sample inside a 10 mm quartz tube measured between 200 and 1100 nm. All our samples selected for the UV-Vis characterization present one region of activity: the $n-\pi^*$ transition in the ultraviolet region around 250–400 nm. This part of the spectrum is dominated by the absorptions from interband transitions, which have been the focus of both fundamental and applied studies due to their possible application in various optical materials [24–31]. For all samples, the low energy of the S11 transition is consistent with large-diameter MWCNTs, and the broadness of the absorption curve is indicative of bundled carbon nanotubes [31].

Now in particular, the 750°C samples show a discrete increase in certain Van Hove singularities (550–800 nm),

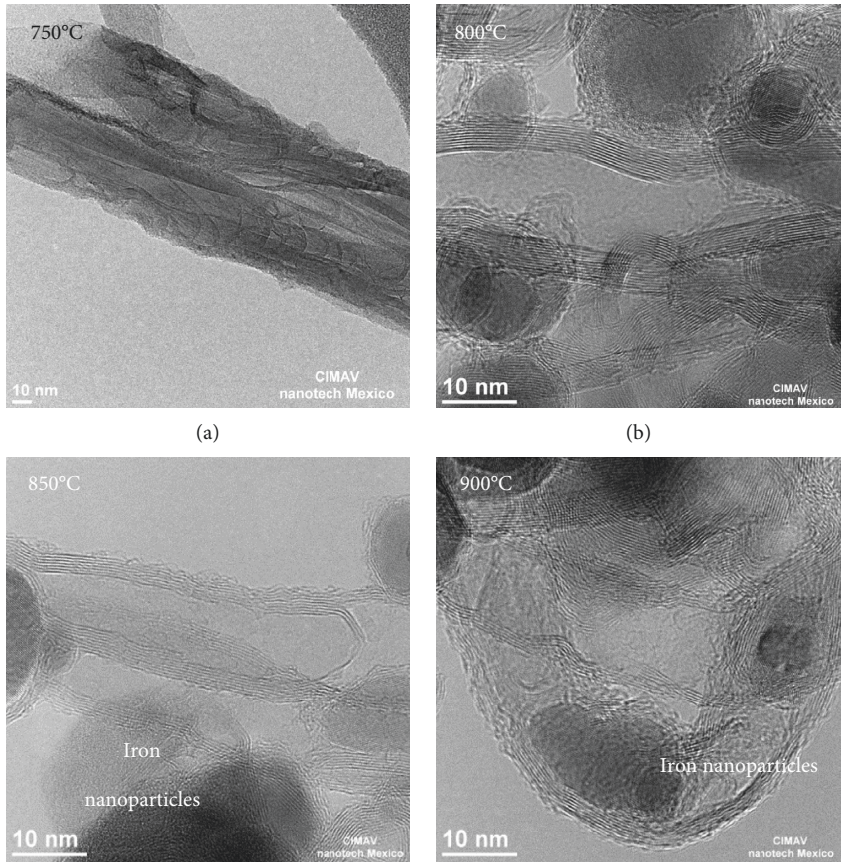

Figure 2: TEM images of CNTs.

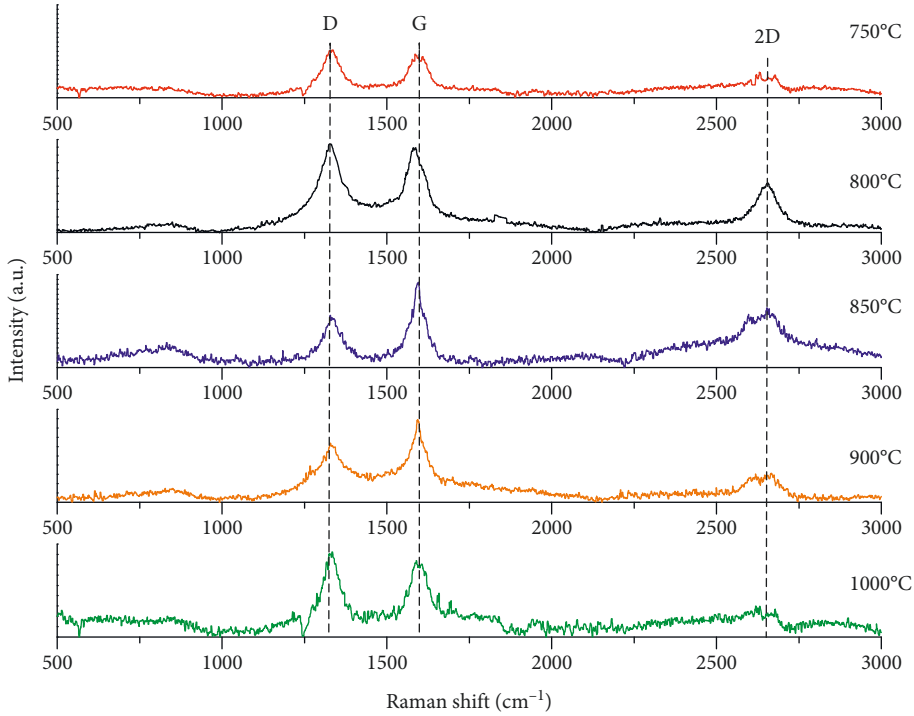

Figure 3: Raman spectra of CNTs.

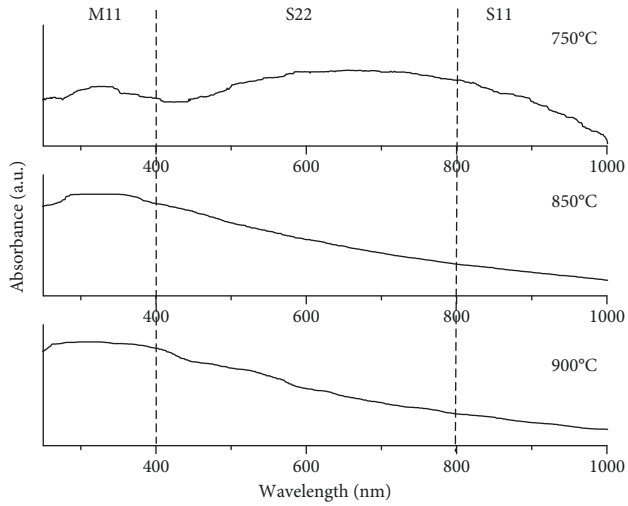

Figure 4: Absorption spectra of 750°C, 850°C, and 900°C, from the visible to near-infrared range.

indicating a possible enrichment of specific diameter semiconducting CNTs [26, 27]. The transitions located in the region S22 for the 850°C and 900°C samples represent a weak presence of Van Hove shifts. These peaks can be attributed to the electronic structure of MWCNTs and can result from electrical conductivity changes and/or structural defects. Additionally from the behavior of the absorption peaks, we can confirm that our samples correspond to MWCNTs samples due to the absorbance increase at the lower wavelength end of the spectra [31].

4. Conclusion

We analyzed the CNTs synthetized through the spray pyrolysis technique using cyclohexanol as a feasible carbon source to grow carbon nanotubes, in a temperature range of 750 to 1000°C. We found a general product increase of 75% with temperature (from 750 to 900°C).

The SEM and TEM images quantitatively show that under our experimental parameters, the ideal temperature to obtain the best product CNTs lies between 800 and 850°C. Outside this temperature, we observe that the obtained CNTs present the appearance of iron impurities, more graphitic carbon, and/or additional structural defects. A quantification of the CNTs /residues ratio could be obtained through thermogravimetry (TGA) or image analysis and it would be performed in the future.

The optical spectroscopy characterization corroborated the presence of $n-\pi^*$ transitions resulting in electrical conductivity changes and several structural defects. Opposing to the literature, the use of cyclohexanol under this synthesis technique and the parameters used did not enhance the crystallinity of CNTs.

Data Availability

The microscopy and spectroscopy data used to support the findings of this study are available from the corresponding author upon request.

Conflicts of Interest

None of the authors of this paper has a financial or personal relationship with other people or organizations that could inappropriately influence or bias the content of the paper.

Acknowledgments

This work has been supported by Centro de Investigaciones en Materiales Avanzados (Center for Research in Advanced Materials (CIMAV)). The technical support of Carlos Ornelas, Wilbert Antunez, and Pedro Pizá and Laboratorio Nacional de Nanotecnología (NANOTECH) is greatly appreciated.

References

[1] S. Abdalla, F. Al-Marzouki, A. A. Al-Ghamdi, and A. Abdel-Daiem, "Different technical applications of carbon nanotubes," *Nanoscale Research Letters*, vol. 10, no. 1, p. 358, 2015.

[2] A. Szabó, E. Kecsenovity, Z. Pápa et al., "Influence of synthesis parameters on CCVD growth of vertically aligned carbon nanotubes over aluminum substrate," *Scientific Reports*, vol. 7, no. 1, p. 9557, 2017.

[3] S. Sakurai, H. Nishino, D. N. Futaba et al., "Role of subsurface diffusion and Ostwald ripening in catalyst formation for single-walled carbon nanotube forest growth," *Journal of the American Chemical Society*, vol. 134, no. 4, pp. 2148–2153, 2012.

[4] A. Shaikjee and N. J. Coville, "The role of the hydrocarbon source on the growth of carbon materials," *Carbon*, vol. 50, no. 10, pp. 3376–3398, 2012.

[5] E. Ordonez-Casanova, M. Roman-Aguirre, A. Aguilar-Elguezabal, and F. Espinosa-Magana, "Characterization of few-walled carbon nanotubes using alcohols aliphatic as carbon source," *Microscopy and Microanalysis*, vol. 19, no. S2, pp. 1608-1609, 2013.

[6] E. G. Ordoñez Casanova, F. Espinosa Magaña, and H. A. Trejo Mandujano, "Theoretical study of electric properties of zigzag carbon nanotubes at low nitrogen concentration," *Results in Physics*, vol. 7, pp. 1230-1231, 2017.

[7] E. Ordoñez-Casanova, M. Román-Aguirre, A. Aguilar-Elguezabal, and F. Espinosa-Magaña, "Synthesis of carbon nanotubes of few walls using aliphatic alcohols as a carbon source," *Materials*, vol. 6, no. 6, pp. 2534–2542, 2013.

[8] S. Musso, G. Fanchini, and A. Tagliaferro, "Growth of vertically aligned carbon nanotubes by CVD by evaporation of carbon precursors," *Diamond and Related Materials*, vol. 14, no. 3–7, pp. 784–789, 2005.

[9] Y. Shirazi, M. A. Tofighy, T. Mohammadi, and A. Pak, "Effects of different carbon precursors on synthesis of multiwall carbon nanotubes: purification and functionalization," *Applied Surface Science*, vol. 257, no. 16, pp. 7359–7367, 2011.

[10] Z.-J. Liu, Z. Xu, Z. Y. Yuan, D. Y. Lu, W. X. Chen, and W. Z. Zhou, "Cyclohexanol dehydrogenation over Co/carbon nanotube catalysts and the effect of promoter K on performance," *Catalysis Letters*, vol. 72, no. 3–4, pp. 203–206, 2001.

[11] Y. Yamamoto, S. Inoue, and Y. Matsumura, "Thermal decomposition products of various carbon sources in chemical vapor deposition synthesis of carbon nanotube," *Diamond and Related Materials*, vol. 75, pp. 1–5, 2017.

[12] A. Aguilar-Elguézabal, W. Antúnez, G. Alonso, F. P. Delgado, F. Espinosa, M. Miki-Yoshida et al., "Study of carbon

nanotubes synthesis by spray pyrolysis and model of growth," *Diamond and Related Materials*, vol. 15, no. 9, pp. 1329–1335, 2006.

[13] I. B. Usman, B. Matsoso, K. Ranganathan, D. Naidoo, N. J. Coville, and D. Wamwangi, "Magnetic properties of aligned iron containing nitrogen-doped multi-walled carbon nanotubes," *Materials Chemistry and Physics*, vol. 209, pp. 280–290, 2018.

[14] N. Saifuddin, A. Z. Raziah, and A. R. Junizah, "Carbon nanotubes: a review on structure and their interaction with proteins," *Journal of Chemistry*, vol. 2013, Article ID 676815, 18 pages, 2013.

[15] Y. Homma, Y. Kobayashi, T. Ogino et al., "Role of transition metal catalysts in single-walled carbon nanotube growth in chemical vapor deposition," *The Journal of Physical Chemistry B*, vol. 107, no. 44, pp. 12161–12164, 2003.

[16] S. Vivekanandhan, M. Schreiber, S. Muthuramkumar, M. Misra, and A. K. Mohanty, "Carbon nanotubes from renewable feedstocks: a move toward sustainable nanofabrication," *Journal of Applied Polymer Science*, vol. 134, no. 4, 2017.

[17] Y. Wang, H. Wei, P. Liu et al., "Effect of structural defects on activated carbon catalysts in catalytic wet peroxide oxidation of m-cresol," *Catalysis Today*, vol. 258, pp. 120–131, 2015.

[18] E. G. Ordonez-Casanova, M. Roman-Aguirre, A. Aguilar-Elguezabal, and F. Espinosa-Magafia, "Structural analysis of carbon nanotubes of various diameters grown by spray pyrolysis using Raman spectroscopy," *Microscopy and Microanalysis*, vol. 21, no. S3, pp. 975-976, 2015.

[19] M. C. Sforna, M. A. Van Zuilen, and P. Philippot, "Structural characterization by Raman hyperspectral mapping of organic carbon in the 3.46 billion-year-old Apex chert, Western Australia," *Geochimica et Cosmochimica Acta*, vol. 124, pp. 18–33, 2014.

[20] G. Gordeev, A. Jorio, P. Kusch et al., "Resonant anti-stokes Raman scattering in single-walled carbon nanotubes," *Physical Review B*, vol. 96, no. 24, article 245415, 2017.

[21] J. Laudenbach, D. Schmid, F. Herziger et al., "Diameter dependence of the defect-induced Raman modes in functionalized carbon nanotubes," *Carbon*, vol. 112, pp. 1–7, 2017.

[22] A. R. Hight Walker, "Resonance Raman spectroscopy of chirality enriched semiconducting carbon nanotubes," in *Proceedings of the APS Meeting Abstracts*, New Orleans, Louisiana, March 2017.

[23] O. Guellati, F. Antoni, M. Guerioune, and D. Bégin, "New doping process mode to synthesize in situ N-MWNTs in novel coaxial nanostructure," *Catalysis Today*, vol. 301, pp. 164–171, 2018.

[24] H. Zhao, X. Liu, Z. Cao et al., "Adsorption behavior and mechanism of chloramphenicols, sulfonamides, and non-antibiotic pharmaceuticals on multi-walled carbon nanotubes," *Journal of Hazardous Materials*, vol. 310, pp. 235–245, 2016.

[25] X. Wei, T. Tanaka, T. Hirakawa et al., "High-yield and high-throughput single-chirality enantiomer separation of single-wall carbon nanotubes," *Carbon*, vol. 132, pp. 1–7, 2018.

[26] A. Tomova, G. Gentile, A. Grozdanov et al., "Functionalization and characterization of MWCNT produced by different methods," *Acta Physica Polonica A*, vol. 6, no. 129, pp. 405–408, 2016.

[27] A. S. K. Kumar, S.-J. Jiang, and W.-L. Tseng, "Effective adsorption of chromium(VI)/Cr(III) from aqueous solution using ionic liquid functionalized multiwalled carbon nanotubes as a super sorbent," *Journal of Materials Chemistry A*, vol. 3, no. 13, pp. 7044–7057, 2015.

[28] S. H. Aboutalebi, A. T. Chidembo, M. Salari et al., "Comparison of GO, GO/MWCNTs composite and MWCNTs as potential electrode materials for supercapacitors," *Energy & Environmental Science*, vol. 4, no. 5, pp. 1855–1865, 2011.

[29] X. Cheng, J. Zhong, J. Meng et al., "Characterization of multiwalled carbon nanotubes dispersing in water and association with biological effects," *Journal of Nanomaterials*, vol. 2011, Article ID 938491, 12 pages, 2011.

[30] I. V. Anoshkin, I. I. Nefedova, D. V. Lioubtchenko, I. S. Nefedov, and A. V. Räisänen, "Single walled carbon nanotube quantification method employing the Raman signal intensity," *Carbon*, vol. 116, pp. 547–552, 2017.

[31] D. Tune and J. Shapter, "Effect of nanotube film thickness on the performance of nanotube-silicon hybrid solar cells," *Nanomaterials*, vol. 3, no. 4, pp. 655–673, 2013.